

COMPUTATION OF LARGE SCALE CURRENTS IN THE ARABIAN SEA DURING WINTER USING A SEMI-DIAGNOSTIC MODEL

C SHAJI¹, N BAHULAYAN², A D RAO¹ AND S K DUBE¹

1. *Centre for Atmospheric Sciences, Indian Institute of Technology, Hauz Khas, New Delhi 110016, India*

2. *Physical Oceanography Division, National Institute of Oceanography, Dona Paula, Goa 403004, India*

(Received 14 October 1996; Revised 3 January 1997; Accepted 11 February 1997)

A 3-dimensional, semi-diagnostic model with 33 levels in the vertical has been used for the computation of climatic circulation in the western tropical Indian ocean. Model is driven with the seasonal mean data on wind stress, temperature and salinity data. Results of numerical experiments for winter season at selected levels are analysed and presented in this paper. The broad features of circulation during winter season such as the westward NEC and SEC, eastward ECC and southward Somali Current is computed successfully by the model. The SEC, NMC and MZC can be seen in all the levels 20, 50, 150 and 300 m depths. Model results show a southward undercurrent at 50 m depth along west coast of India, a southward subsurface current off Somali near 5° N at 150 and 300 m depths. Computed circulation features at the surface and subsequent levels showed fairly good agreement with the observations.

Key Words: Semi-diagnostic model; 3-Dimensional; Leap-frog Circulation; Thermohaline forcing

Introduction

Indian ocean, especially one of its marginal seas Arabian Sea, plays a very significant role in regulating the monsoons over the Indian subcontinent. The large scale air-sea interaction processes on monthly, seasonal and intra-seasonal time scales in the Arabian Sea are mainly controlled by basin scale 3-dimensional circulation which generates temperature and salinity inhomogeneities in the sea and modifies the heat budget parameters at the air-sea interface. To understand the dynamics that control the temperature and salinity variability and to predict the warming and cooling processes in the Arabian Sea, it is first essential to model the 3-dimensional climatic circulation which would serve as initial conditions in prognostic models of ocean circulation.

Semi-diagnostic ocean circulation models are effective tools to compute the climatological mean circulation and to understand the role of local forces in driving the circulation. The concept and basic approach to semi-diagnostic modelling were first developed by Marchuk and Sarkisyan.¹ A few simplified semi-diagnostic models have been developed for the circulation of large scale circulation in the world oceans^{2,3}.

In the present study, a 3-D semi-diagnostic circulation model is used to study the climatic circulation in the western tropical Indian Ocean during winter season.

Model Equations

The model (20°S-30°N and 35°E-80°E) used for this study has 33 levels in the vertical, a resolution of 1° in the zonal and meridional directions. The model equations are based on the basic hydrothermodynamic equations in spherical co-ordinate system governing the large scale 3-dimensional circulation in the ocean given by Gill.⁴ These equations are then modified in terms of colatitude of the place and particular sign convention used in the model wherein the longitude (λ) increases towards east, the colatitude (θ) increases towards south and vertical co-ordinate (z) increases downwards. The final model equations assuming approximations of Boussinesq, hydrostatics and incompressibility of sea water are :

$$\frac{\partial u}{\partial t} + Au + lv + \cot\theta \frac{uv}{R} = -\frac{1}{\rho_0 R \sin\theta} \frac{\partial p}{\partial \lambda} + F\lambda \quad \dots(1)$$

$$\frac{\partial v}{\partial t} + Av - lu - \cot\theta \frac{u^2}{R} = -\frac{1}{\rho_0 R} \frac{\partial p}{\partial \theta} + F\theta \quad \dots(2)$$

$$\frac{\partial \rho}{\partial z} = g\rho \quad \dots(3)$$

$$\frac{1}{R \sin\theta} \left[\frac{\partial u}{\partial \lambda} + \frac{\partial(v \sin\theta)}{\partial \theta} \right] + \frac{\partial w}{\partial z} = 0, \quad \dots(4)$$

$$\rho = \rho(T, S), \quad \dots(5)$$

$$\frac{\partial T}{\partial t} + AT = \frac{\partial \left[v_T \frac{\partial T}{\partial z} \right]}{\partial z} + \mu_T \Delta T \quad \dots(6)$$

and

$$\frac{\partial S}{\partial t} + AS = \frac{\partial \left[v_T \frac{\partial S}{\partial z} \right]}{\partial z} + \mu_T \Delta S \quad \dots(7)$$

where

- θ - co-latitude = $90-\phi$, ϕ is the latitude.
- u, v, w - the velocity components along the east (λ), south (θ) and downward (z) directions respectively
- p - hydrostatic pressure
- ρ - density of sea water
- ρ_0 - constant density
- R - radius of the Earth
- l - $2\Omega \cos\theta$
- Ω - angular velocity of Earth's rotation
- Au, Av - advective acceleration terms
- F, F^0 - friction terms in the momentum equations
- μ, ν - horizontal and vertical turbulent mixing coefficients respectively
- μ, ν - horizontal and vertical turbulent diffusion coefficients of heat and salt
- T - temperature
- and S - salinity

$$Af = \frac{1}{R \sin\theta} \left[\frac{\partial(uf)}{\partial\lambda} + v \frac{\partial(f \sin\theta)}{\partial\theta} \right] + \frac{\partial(wf)}{\partial z}$$

$$F^\lambda = \frac{\partial \left(v \frac{\partial u}{\partial z} \right)}{\partial z} + \mu \left[\Delta u - \frac{u}{R^2 \sin^2\theta} + \frac{2 \cos\theta}{R^2 \sin^2\theta} \right] \frac{\partial v}{\partial \lambda}$$

$$F^\theta = \frac{\partial \left(v \frac{\partial v}{\partial z} \right)}{\partial z} + \mu \left[\Delta v - \frac{v}{R^2 \sin^2\theta} + \frac{2 \cos\theta}{R^2 \sin^2\theta} \right] \frac{\partial u}{\partial \lambda}$$

$$\Delta f = \frac{1}{R^2 \sin^2\theta} \frac{\partial^2 f}{\partial \lambda^2} + \frac{1}{R^2 \sin\theta} \frac{\partial(\sin\theta \frac{\partial f}{\partial \theta})}{\partial \theta}$$

Boundary Conditions

At the ocean surface ($z=0$), the following boundary conditions were used.

$$\rho_{0,v} \frac{\partial u}{\partial z} = -\tau_{\lambda}; \rho_{0,v} \frac{\partial v}{\partial z} = -\tau_{\theta}; w|_{z=0} = 0; T|_{z=0} = T^*; S|_{z=0} = S^*, \quad \dots(8)$$

where τ_{λ} and τ_{θ} are the components of wind stress in the zonal and meridional directions respectively; u, v are the velocity components and T and S are the observed temperature and salinity data at the surface.

Non-slip boundary condition for velocity fields is applied at the bottom $z=H(\lambda, \theta)$

$$\text{i.e., } u = v = w = 0 \quad \dots(9)$$

$$\frac{\partial T}{\partial z} = \frac{\partial S}{\partial z} = 0 \quad \dots(10)$$

The normal flux boundary conditions of zero velocity is prescribed at the lateral boundaries,

$$\text{i.e., } V_n = 0 \quad \dots(11)$$

and

$$\frac{\partial T}{\partial n} = \frac{\partial S}{\partial n} = 0, \quad \dots(12)$$

where 'n' is the normal to the boundary.

At the open sea boundaries, the velocity components computed with the help of quasi-geostrophic model of Marchuk and Sarkisyan¹ were used.

The temperature and salinity at the open sea boundaries were given as :

$$T|_l = T^*; S|_l = S^*, \quad \dots(13)$$

where T^* and S^* are climatic temperature and salinity data.

Initial Conditions

An initial state of rest is prescribed at time $t = 0$.

$$(u, v)_{t=0} = 0; (T, S)_{t=0} = (T^*, S^*) \quad \dots(14)$$

By writing the density of sea water ' ρ ' as the sum of the average density ' ρ_0 ' and the density anomaly ρ' (λ, θ, z) and integrating the hydrostatic eq. (3) in the vertical from free surface to depth z , the hydrostatic pressure at depth z becomes :

$$P_z = \rho_0 g \zeta + g \int_0^z \rho' dz, \quad \dots(15)$$

where ' ζ ' is the sea surface topography or sea level. An additional equation for sea surface topography (sea level) has to be derived to have a closed system of 8 model equations in 8 unknown variables.

Sea Surface Topography Equation

Eqs. (1)-(5) are solved by means of a leap-frog numerical scheme. By adding the equation of continuity along all levels after considering the boundary condition at the surface and bottom for vertical velocity (i.e., $w=0$), the two-dimensional integral continuity equation which is the equation for sea surface topography at the internal grid points is obtained. By applying the lateral boundary condition for velocity field in the two-dimensional integral continuity equation, the sea level equation at the boundary points are also obtained. The sea level equation at the internal grid point is :

$$\frac{1}{R \sin \theta} [\delta_\lambda u^\theta + \delta_\theta \overline{v \sin \theta}^\lambda] = 0, \quad \dots(16)$$

where δ_λ and δ_θ are the finite difference operators and u and v are the vertically integrated velocity components in the zonal and meridional direction respectively. Substituting the values of u and v in the integral continuity equation, the final expression for sea surface topography is written as follows:

$$\frac{1}{R \sin \theta} [\delta_\lambda (a \delta_\lambda \zeta^{-\theta} + b \delta_\theta \zeta^{-\lambda})^\theta + \delta_\theta (a \delta_\theta \zeta^{-\lambda} - b \delta_\lambda \zeta^{-\theta})^\lambda \sin \theta] = R_s, \quad \dots(17)$$

where

$$a = \frac{\Delta t g H}{1 + \left(\frac{\Delta t^2 l^2}{4} \right)},$$

$$b = a l \frac{\Delta t}{2},$$

$$R_s = \frac{1}{R \sin \theta} \left[\delta_\lambda \overline{R_\lambda \theta} + \delta_\theta (\overline{R_\theta \lambda} \sin \theta) \right],$$

$$R_\lambda = R_u - \left(\frac{\frac{\Delta t l}{2} R_v}{1 + \frac{\Delta t^2 l^2 \rho}{4}} \right),$$

$$R_\theta = R_v + \left(\frac{\frac{\Delta t l}{2} R_u}{1 + \frac{\Delta t^2 l^2 \rho}{4}} \right),$$

$$R_u = u^{n-1} + \Delta t \left[-\frac{lu^{n-1}}{2} - \left(\frac{g}{\rho_0 R \sin \theta} \int_0^z \frac{\partial \rho'}{\partial \lambda} dz - Au - \cot \theta \frac{uv}{R} \right)^n + (F^\lambda)^{n-1} \right]$$

and

$$R_v = v^{n-1} + \Delta t \left[-\frac{lv^{n-1}}{2} - \left(\frac{g}{\rho_0 R} \int_0^z \frac{\partial \rho'}{\partial \theta} dz - Av - \cot \theta \frac{u^2}{R} \right)^n + (F^\theta)^{n-1} \right],$$

where Δt is the time step and n is the time step number.

The sea surface topography eq. (17) is solved by successive overrelaxation technique.

Numerical Experiments and Results

In the semi-diagnostic method, the steady state solution of model equations is obtained in two stages on a 46x51 staggered grid. In the first stage, all the equations except turbulent diffusion equations of heat and salt are solved subject to proper boundary and initial conditions mentioned above. The integration of the equations is continued for approximately 20 days to obtain a quasi-steady solution for velocity field. The density is kept constant in this stage. In the second stage, the diagnostic equations together with the turbulent diffusion equations of heat and salt are again

solved using the velocity field obtained during the first stage and original temperature and salinity fields as initial conditions. The integration of the complete set of model equations is again continued for another 20 days to achieve a steady state solution. The total period of integration for both the stages is 40 days. A value of $5 \times 10^8 \text{ cm}^2 \text{ sec}^{-1}$ is used for the horizontal eddy viscosity (μ) and eddy diffusivity (μ_v) coefficients in the model, whereas the vertical eddy viscosity (ν) and eddy diffusivity (ν_v) coefficients consider a value of $10 \text{ cm}^2 \text{ sec}^{-1}$.

Model Input

The model is driven with the wind stress at the sea surface and thermohaline field at various levels. The wind stress data for the winter (average of December, January and February months) season used in the present study is obtained from Hellerman and Rosenstein⁵. Since the model resolution is 1° in the zonal and meridional directions, the original wind data compiled by Hellerman ($2^\circ \times 2^\circ$) have been interpolated to 1° resolution by means of a bilinear interpolation technique for the model area (20° S - 30° N and 35° E - 80° E). In order to provide thermohaline forcing, the temperature and salinity data is obtained from the climatology of Levitus⁶.

Results and Discussion

Results of numerical experiments at 20, 50, 150 and 300 metres depths in the upper levels of the ocean is discussed here. Fig. 1 shows the distribution of resultant wind field in the study area during winter season. Arabian sea north of the equator is covered mainly by northeasterly winds. In the doldrums region near the equator, the wind field is very weak except off Somali and African coasts. Southeasterly winds with magnitudes greater than 1 dynes cm^{-2} are observed in the Southern Hemisphere between 10° S and 20° S latitude.

Figs. 2 (a-d) represent the σ_t fields at 20, 50, 150 and 300 metres depths. At 20m and 50m depths, σ_t fields decreases gradually from north to south. Low dense water is found off the south west coast of India at these depths. At 150m and 300m depths, high dense water is found in the northern Arabian Sea and these high dense waters can be seen between 5° S and 10° S latitude. The σ_t lines are more or less oriented in a zonal direction between 10° S and 20° S latitude at these depths.

Computed Circulation and Sea Surface Topography

Figs. 3 (a-d) represent the model computed currents at 20, 50, 150 and 300 metres depths. Model computed sea surface topography is presented in Fig. 4. There is very weak southwesterly flow in the Arabian Sea north of 15° N due to the combined effect of wind stress and thermohaline forcing. The westward flowing North Equatorial Current (NEC) ranges between the equator and 10° N latitude. At the northern tip of Somali, NEC branches into two; one flowing north and the other flowing as the

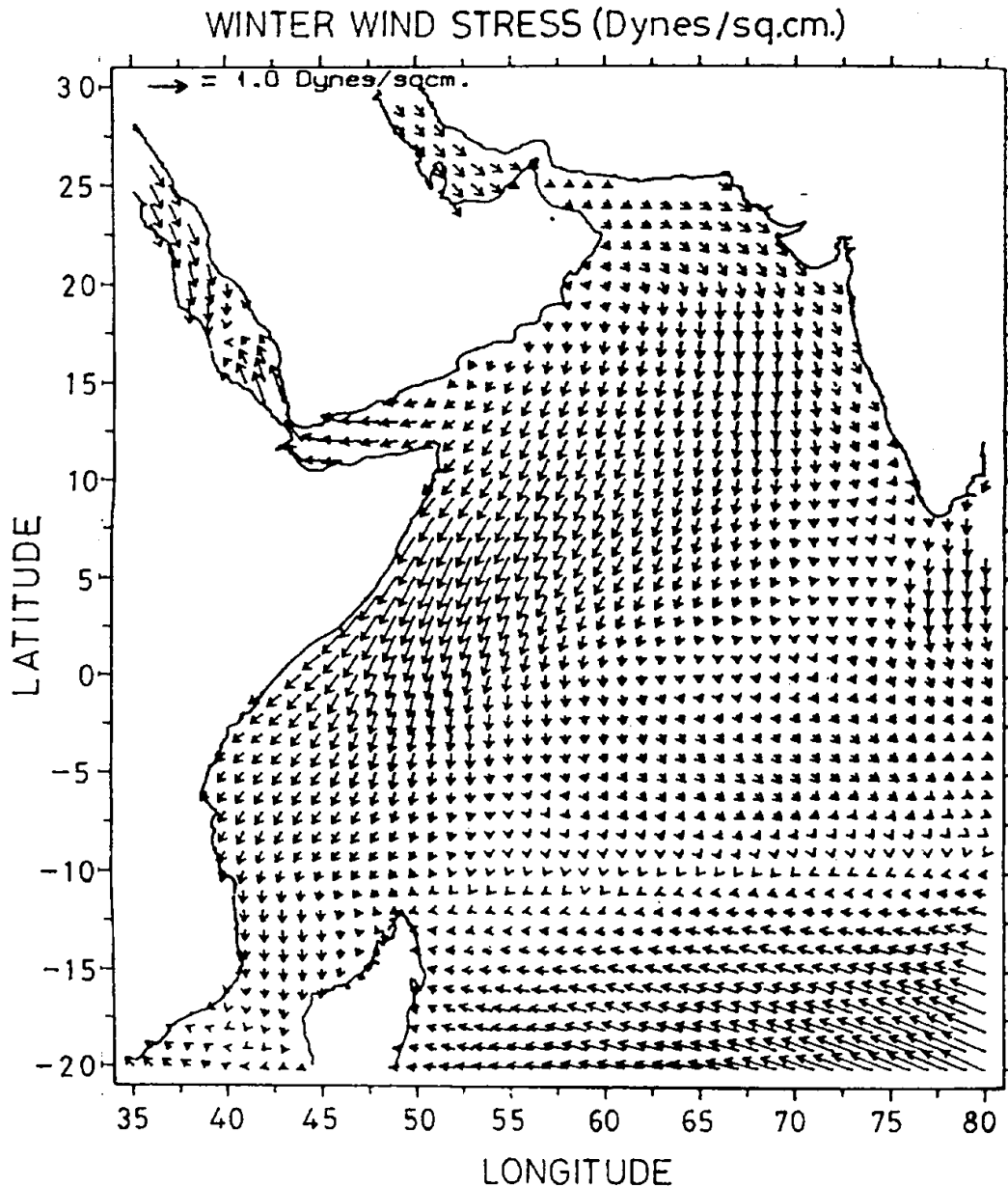


Fig 1 Observed mean resultant wind stress (dynes cm^{-2}) during winter

southward Somali Current (Sc) all along the Somali coast. The Southward Somali Current attains a maximum velocity of 75 cm Sec^{-1} . South Equatorial Current (SEC) is observed approximately between 10° S and 20° S latitudes. The intensity of SEC is diminished from south to north. The eastward Equatorial Counter Current (ECC), jointly fed by the southward SC and SEC is found in the Southern Hemisphere between 3° S and 8° S east of 50° E . The SEC turns southward at the northern tip of Madagascar to form the broad southward flowing western boundary current namely the Mozambique Current (MZC). The sea surface topography contours are well packed in the SEC and North Madagascar Current (NMC) region (Fig 4). The

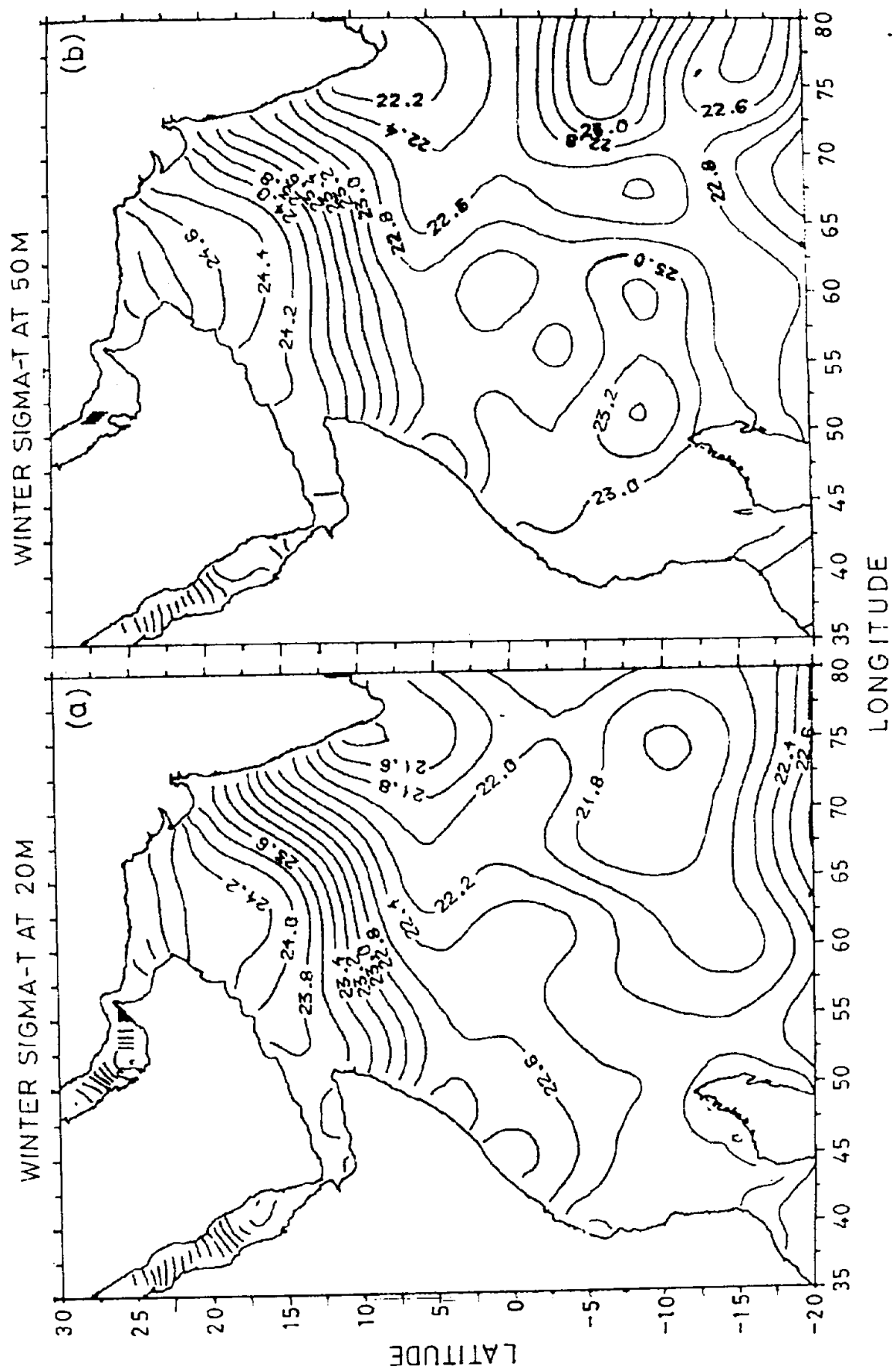


Fig 2 Spatial distribution of σ during winter at (a) 20m depth (b) 50m depth

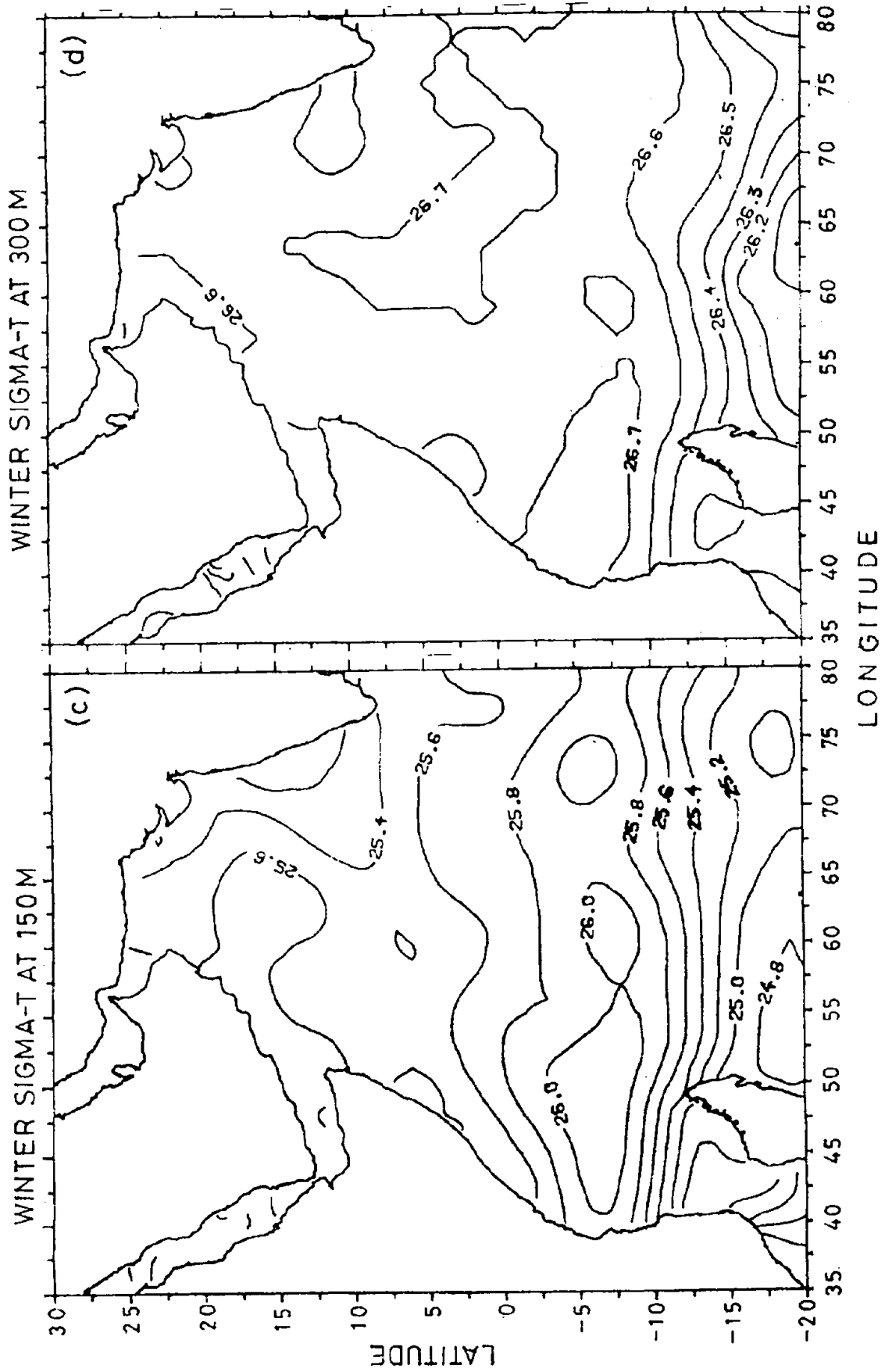


Fig 2 Spatial distribution of σ_t during winter at (c) 150m depth and (d) 300m depth

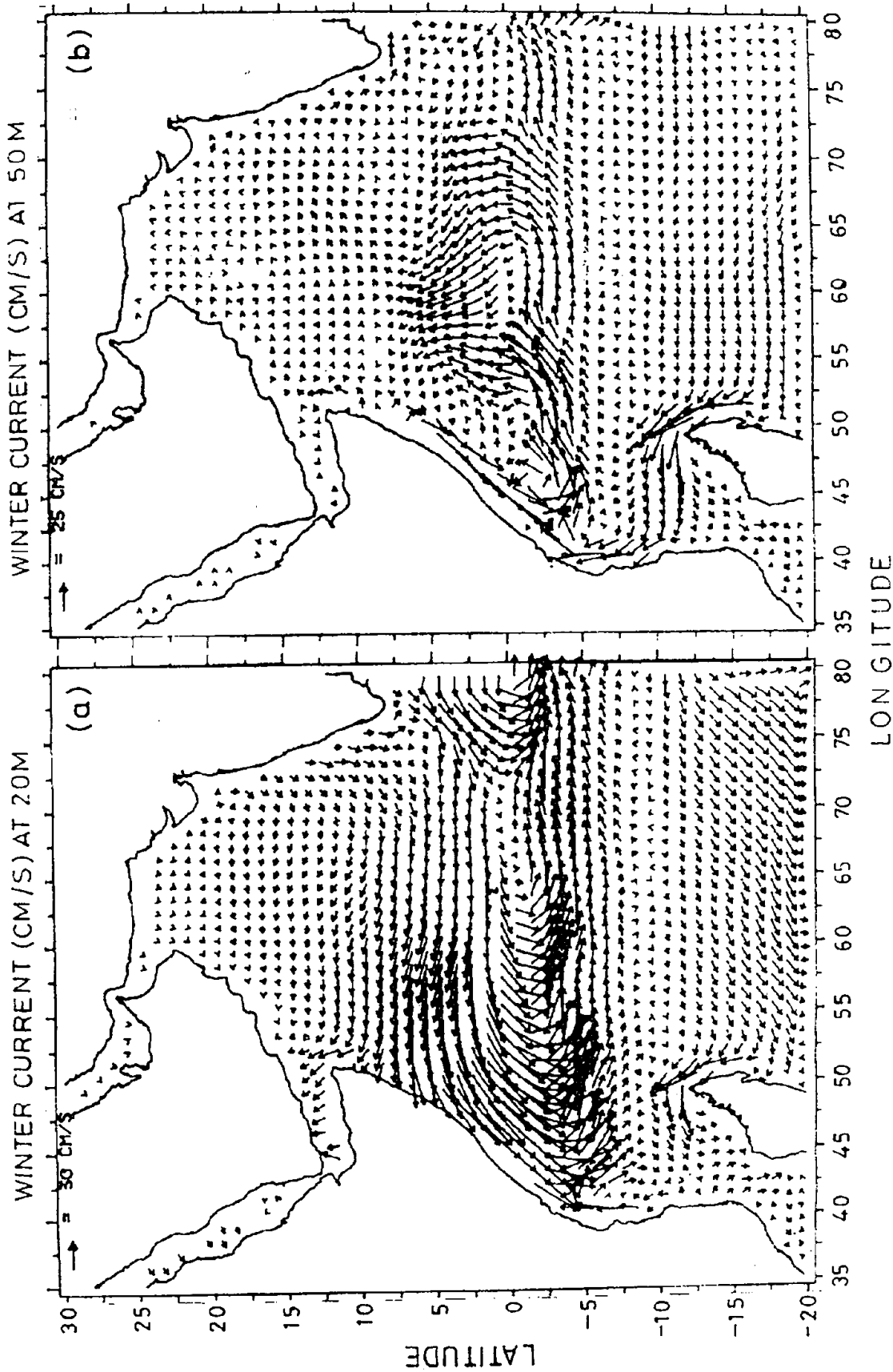


Fig 3 Computed circulation during winter season at (a) 20m depth (b) 50m depth

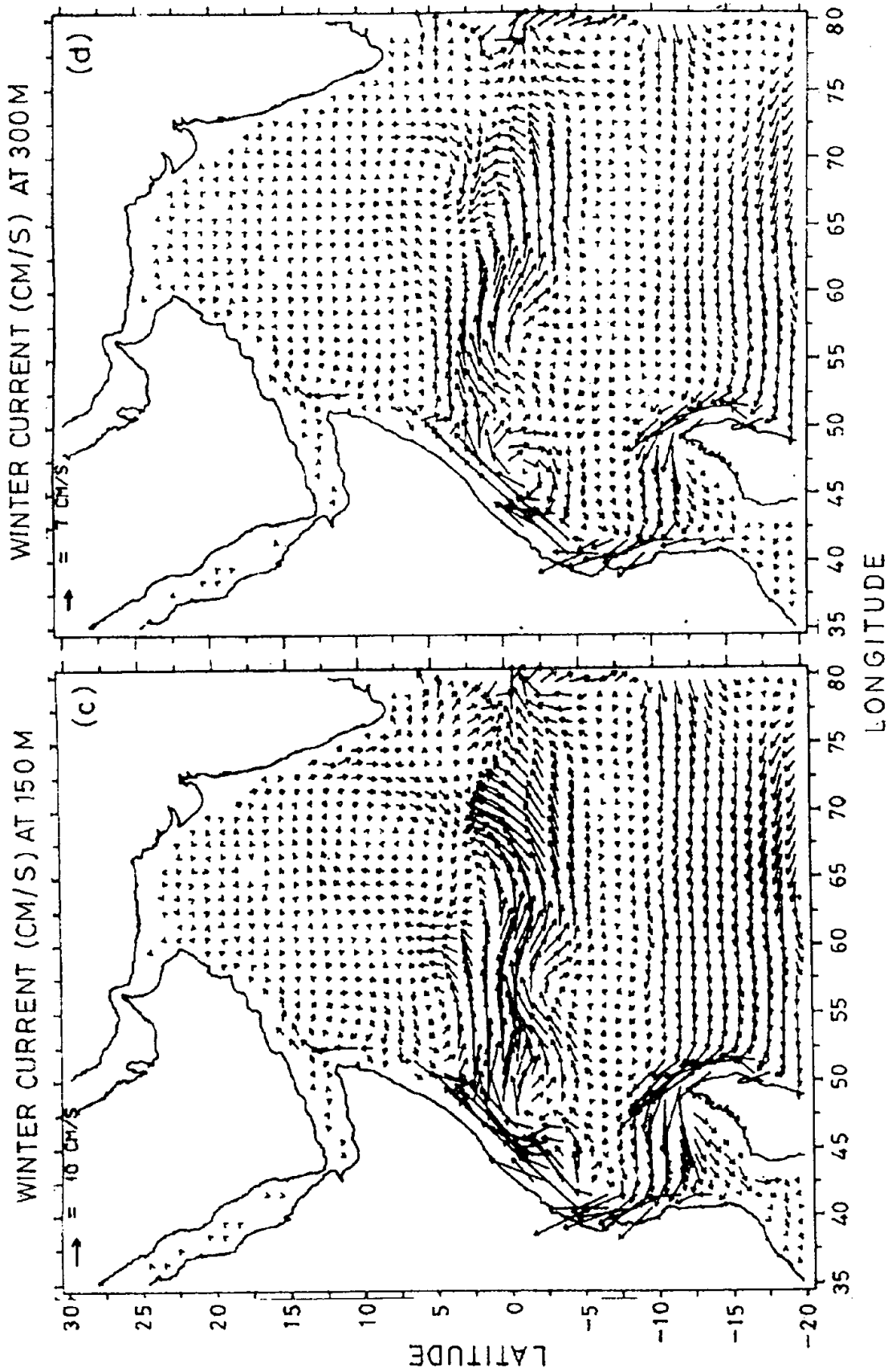


Fig 3 Computed circulation during winter season at (c) 150m depth (d) 300m depth

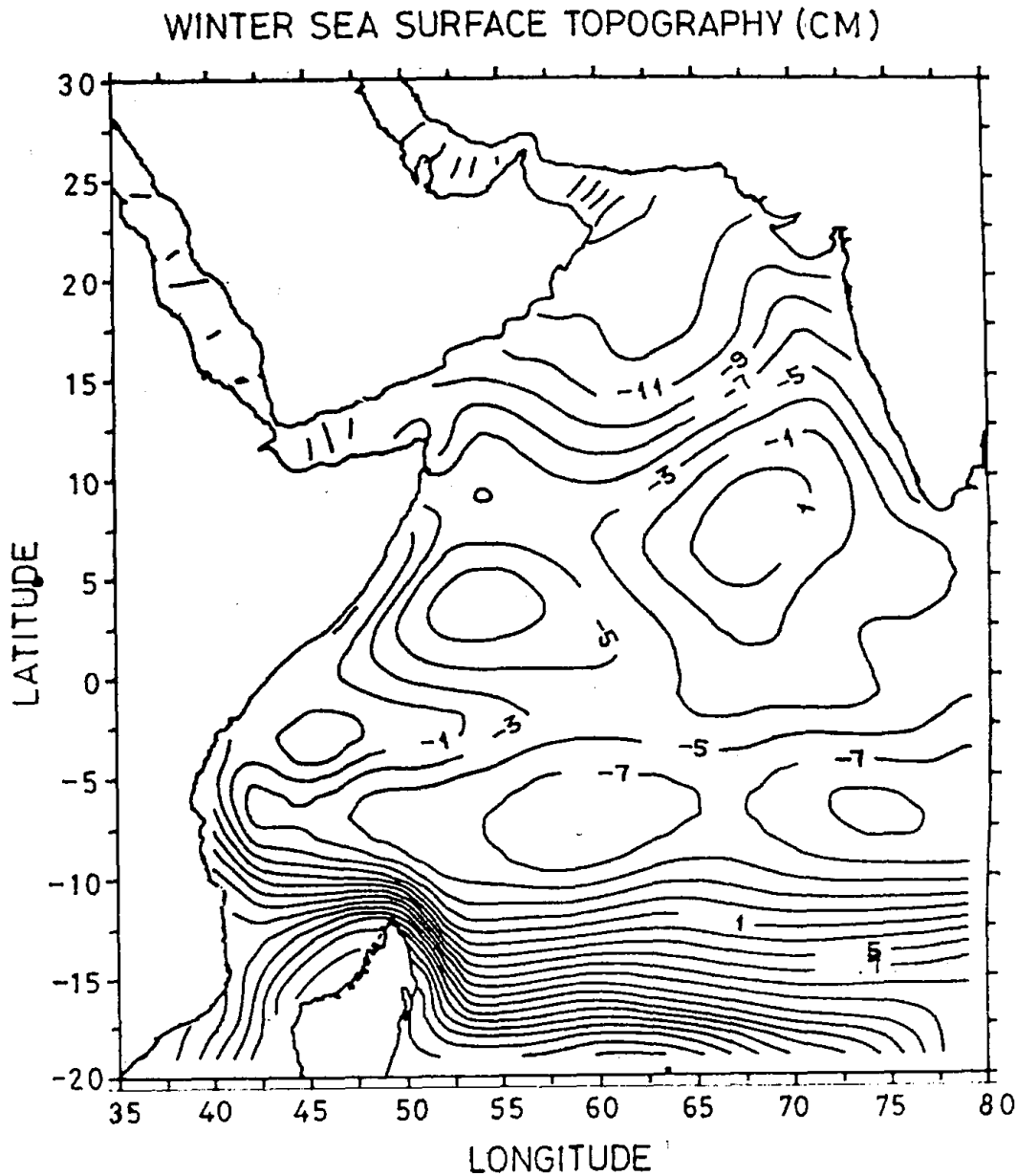


Fig 4 Computed sea surface topography (cm) during winter season

topography contours show the presence of SEC, NMC, MZC, ECC and EACC in the southern tropical Indian Ocean at the surface level. These results are consistent with the ship drift climatology compiled by Cutler and Swallow⁷.

The circulation pattern at 50m depth (Fig 3b) has changed in the Northern Hemisphere except off Somali and Indian coasts. There is no remarkable change of flow in the Southern Hemisphere where SEC, NMC, MZC and East African Coastal Current (EACC) is still persisting. An eastward Equatorial Under Current (EUC) is found in the Southern Hemisphere between 2°S and 7°S, east of 45°E longitude. The

model results shows a weak southward undercurrent at 50 m depth along southwest coast of India, in consistent with the southward undercurrent reported by Shetye *et al.*⁸ in their hydrographic survey. The southeastern sector of the Arabian Sea is covered by an anticyclonic gyre circulation.

At 150 m and 300 m depths (Fig.3(c-d)), the flow direction has changed along the African coasts; the northward flowing EACC penetrated more towards north and reached upto the southern Somalia coast. The SEC, NMC and MZC is also seen at their respective locations in these depths. There is outflow of high saline waters from the Red Sea towards Cenral Arabian Sea and along the Arabian coasts at 150m and 300 m depths, which is significant from the high σ_t values observed in these regions. The anticyclonic gyre observed at 50m depth in the south central Arabian Sea is seen at 150m and 300 m depths also. The current measurements of Quadfasel and Schott⁹ reported a southward flowing subsurface current off Somali near 5° N. The same flow is seen in the model results also at these depths.

Acknowledgements

Authors are grateful to the Head, Centre for Atmospheric Sciences, IIT, New Delhi and Head, Data Division, NIO, Goa for facilities. The computations were carried out in the AVIION-4000 computer at the Data Division, NIO, Goa and the co-operation rendered by the staff of the Division are gratefully acknowledged. One of the authors (C Shaji) is grateful to the CSIR, New Delhi for awarding a Senior Research Fellowship to carry out this work.

References

- 1 G I Marchuk and A S Sarkisyan *Mathematical Modelling of Ocean Circulation* Springer-Verlag Berlin (1988) 292 pp
- 2 A S Sarkisyan and Yu L Demin *Large Scale Oceanographic Experiments WCRP Pub. Tokyo* 2 (1) (1983) 201-214
- 3 Yu L Demin and R A Ibraev *Sov J Num Anal Math Modelling* 4 (3) (1989) 211-225
- 4 A E Gill *Atmosphere-Ocean Dynamics* Academic Press New York (1982) 662 pp
- 5 S Hellerman and M Rosenstein *J Phys Oceanogr* 13 (1983) No. 7 1093-1104
- 6 S Levitus *Climatological Atlas of the World Ocean. NOAA prof pap. 13 US Govt Ptg Off Washington D C* (1982) 173 pp
- 7 A N Cutler and J C Swallow *Surface Currents of the Indian Ocean Institute of Oceanographic Sciences U K* (1984) 8 pp
- 8 S R Shetye, A D Gouveia, S S C Sheno, G S Michael, D Sundar, A M Almeida and K Santanam *Deep-Sea Res* 38 (1991) 1517-1529
- 9 D R Quadfasel and F Schott *J geophys Res* 88 C10 (1983) 5973-5979